

3D-GMNet: Learning to Estimate 3D Shape from A Single Image As A Gaussian Mixture

Kohei Yamashita Shohei Nobuhara Ko Nishino
Graduate School of Informatics, Kyoto University

Abstract

In this paper, we introduce 3D-GMNet, a deep neural network for single-image 3D shape recovery. As the name suggests, 3D-GMNet recovers 3D shape as a Gaussian mixture model. In contrast to voxels, point clouds, or meshes, a Gaussian mixture representation requires a much smaller footprint for representing 3D shapes and, at the same time, offers a number of additional advantages including instant pose estimation, automatic level-of-detail computation, and a distance measure. The proposed 3D-GMNet is trained end-to-end with single input images and corresponding 3D models by using two novel loss functions: a 3D Gaussian mixture loss and a multi-view 2D loss. The first maximizes the likelihood of the Gaussian mixture shape representation by considering the target point cloud as samples from the true distribution, and the latter improves the consistency between the input silhouette and the projection of the Gaussian mixture shape model. Extensive quantitative evaluations with synthesized and real images demonstrate the effectiveness of the proposed method.

1 Introduction

Single-image 3D reconstruction has a wide variety of applications including AR, robotics, and autonomous driving. For example, image-based 3D estimation can provide an initial guess to grasp targets for robots and to avoid obstacles for autonomous vehicles. Similarly, it can provide cues for inter-frame egomotion estimation [26] as well as for superimposing synthetic objects into the real world.

Image-based 3D reconstruction is, in general, an ill-posed problem. As a 2D image is a projection of the 3D

scene, the recovery of the original 3D information from this degenerated observation is generally not unique. For this, past methods have leveraged constraints arising from projective geometry [1, 10, 23, 24], radiometric surface properties [2, 3, 12], and optical imaging properties [8, 18].

Recently, convolutional neural networks have been widely used to devise prior knowledge of the target 3D shape for these 3D shape estimation problems. By using a sufficient number of paired training data of 3D shapes and their 2D appearances [5], recent works [6, 7, 13, 16, 29] have shown that 3D geometry recovery from a single image can be learned end-to-end.

In this paper, we introduce a novel single-image 3D shape recovery network that outputs a compact, analytical model with a number of advantages over conventional representations, namely point clouds, voxels, and mesh models. The key idea is to model the 3D shape with a Gaussian mixture (Figure 1). For this, 3D shape recovery is formulated as kernel density estimation, *i.e.*, 3D shape reconstruction as estimation of a 3D probability distribution that generates the target point cloud. The resulting 3D Gaussian mixture shape representation significantly reduces memory footprint compared to voxel-based occupancy estimation approaches [6, 31] and also provides a straightforward means for defining the surface in contrast to unstructured point cloud representation [7, 13]. Also in sharp contrast to mesh-based shape representations, the Gaussian mixture model enables the network to adaptively refine the shape topology.

To recover the 3D shape from a single image as a 3D Gaussian mixture model, we introduce a novel deep neural network which we refer to as 3D-GMNet. Given a single image as an input and its corresponding 3D shape as the supervision, the proposed network learns to out-

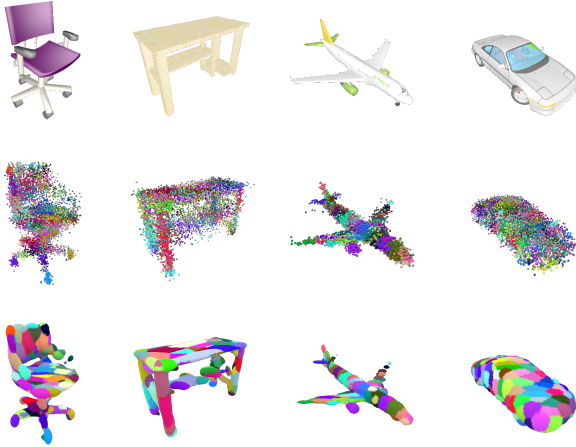


Figure 1: We introduce a novel deep neural network called 3D-GMNet. From a single image (first row), recovers 3D shape as a 3D Gaussian mixture (second row: shown as sampled distribution, third row: shown as a surface at constant variance). The resulting shape representation is extremely compact, and offers additional benefits such as direct distance and pose measures.

put a set of parameters that define the Gaussian mixture shape model. We propose two novel loss functions to train 3D-GMNet end-to-end. The first is the 3D Gaussian mixture loss, which evaluates the accuracy of the estimated Gaussian mixture model with regards to the target 3D shape. This is achieved by maximizing the likelihood of the Gaussian mixture which in turn is evaluated by considering the target 3D points as samples from the true distribution. The second is the multi-view 2D loss that evaluates the accuracy of the 2D projections of the Gaussian mixture to random viewpoints against the true silhouettes, *i.e.*, the projections of the ground truth 3D shape to the same viewpoints.

The recovered 3D Gaussian mixture shape model has a number of advantages over conventional 3D shape representations. Most important, it is compact as it requires only the 3D mean and covariance for each mixture component. In addition, it admits a number of direct favorable applications, including automatic level-of-detail computation via Gaussian mixture reduction, pose estimation, and distance measurement. We demonstrate these properties, in particular in the context of pose alignment and level-of-detail computation, together with the effective-

ness of 3D-GMNet with a number of synthetic and real images. The results show that 3D-GMNet recovers accurate 3D shape from a single image with a representation that opens a new avenue of use in fundamental applications.

2 Related Work

Shape Representation Learning-based 3D shape estimation studies can be categorized by their shape representations: voxel-grid [6,31], point clouds [7,13], patches [9], mesh models [14,29], primitive sets [19,21,27], or learned function [17,20].

Wu *et al.* [31] discretize the target 3D shape into a $128 \times 128 \times 128$ voxel grid and their neural network estimates the occupancy of each voxel. This is a memory-intensive approach, although it can handle 3D shapes of different topology in a unified manner.

Point cloud approaches represent the target 3D shape as a collection of 3D points on the object surface. Lin *et al.* [16] propose a network that estimates multi-view depth-maps from a single image. They fuse the multi-view depth-maps and project it to 2D image planes for jointly optimizing a depth and a silhouette loss function. Groueix *et al.* [9] represents the target 3D shape by a collection of 3D patches. Although memory efficient, fusing multiple depth-maps or multiple patches into a single watertight 3D shape remains challenging.

Mesh-based approaches [14,29] can make use of local connectivity of the 3D shape. Handling different topologies, however, becomes an inherently challenging task with meshes. Primitive-based approaches [19,21,27] represent the target 3D shape as a collection of simple objects such as cuboids or superquadrics. They can realize a compact representation of the target volume, but cannot represent smooth and fine structures by definition.

Mescheder *et al.* [17] train the network as a nonlinear function representing the occupancy probability of 3D object shape. For a given 3D position, the network infers the probability of being part of the object volume. This approach is highly scalable in resolution. Compared with voxel-grid approaches whose networks are trained for specific voxel resolutions, it can sample 3D points as dense as required. On the other hand, it is a computation-intensive shape representation since the network should

infer the probability for each and every sample.

Our Gaussian mixture-based representation has the advantages of these representations. It models not only the surface points but also the interior of the volume, with an efficient parameterization, *i.e.*, a set of Gaussian parameters, and can generate a watertight 3D surface of arbitrary resolution as its isosurface. This can be seen as a probability density approach with Gaussian distributions, and also as a primitive-based approach with Gaussians as primitives. Additionally, in contrast to cuboid-based approaches, our shape representation can realize 3D registration with a simple algorithm as described in Section 4.2.

Neural Networks for Mixture Density Estimation

Mixture density network [4] is a method to predict a target multimodal distribution as a mixture density distribution. Bishop [4] introduced this network architecture with isotropic Gaussian basis functions. Williams extended it to utilize a general multivariate Gaussian distribution as the basis function [30]. As describe in Section 3.2, our density estimation network is inspired by these works.

Loss Functions When training deep neural networks for 3D shape estimation, most existing studies use combinations of a 3D shape loss, a multi-view 2D loss and an adversarial loss. The 3D shape loss evaluates the difference between the predicted and the target shapes. Choy *et al.* [6] used the cross entropy for a voxel-grid representation. Chamfer distance can measure the distance to the target shape from point clouds [7, 13] or mesh models [29]. When using mesh representations, consistencies of surface normals and edge lengths in 3D can also be used.

Multi-view 2D consistency evaluates the difference between the 2D projection of the predicted shape and its ground truth such as silhouettes [13, 14, 33] or depth-maps [16]. Adversarial training is also used to make the predicted shapes plausible [13]. Jiang *et al.* [13] proposed a discriminator that classifies whether the 3D shape is a predicted one or a true one based on semantic features extracted from the 3D shape and the 2D input image. In this paper, we introduce 3D shape and multi-view 2D losses that take full advantage of statistical and geometric properties of 3D Gaussian distributions.

3 3D Gaussian Mixture Network

Figure 2 shows an overview of our 3D-GMNet. Given a 2D image of an object, our 3D-GMNet estimates a set of parameters that defines a Gaussian mixture that best represents the 3D shape of the object in the input image.

In this section, we first introduce the Gaussian-mixture 3D shape representation (Section 3.1), and then the proposed network for estimating its parameters from an image (Section 3.2) using a 3D shape loss (Section 3.3) and a multi-view 2D loss (Section 3.4).

3.1 3D Shape as A Probability Density Function

Our key idea is to consider the target 3D volume as a collection of observations of a random variable with a Gaussian mixture distribution. Suppose a ground-truth 3D shape is given as a collection of 3D point cloud. We assume that this 3D point cloud samples the object volume, which can easily be computed from the 3D models from the training data. As such, we may regard them as voxels, too. Each one of the voxels is a sample of the random variable, and our goal when training the network is to estimate a Gaussian mixture distribution that describes these samples best.

We assume that the density is uniform in the object and normalized. The density function $f(\mathbf{x})$ is described as

$$f(\mathbf{x}) = \begin{cases} \frac{1}{V} & \text{inside the object,} \\ 0 & \text{otherwise,} \end{cases} \quad (1)$$

where \mathbf{x} is a 3D position and V is volume of the object.

3D Gaussian Mixture Distribution We use a 3D Gaussian mixture to approximate the true distribution $f(\mathbf{x})$. A 3D Gaussian distribution is defined as

$$\phi(\mathbf{x}|\boldsymbol{\mu}, \boldsymbol{\Sigma}) = \frac{1}{(2\pi)^{\frac{3}{2}}|\boldsymbol{\Sigma}|^{\frac{1}{2}}} \exp\left(-\frac{1}{2}g(\mathbf{x}|\boldsymbol{\mu}, \boldsymbol{\Sigma})\right), \quad (2)$$

where $\boldsymbol{\mu}$ is the mean, $\boldsymbol{\Sigma}$ is the covariance matrix and

$$g(\mathbf{x}|\boldsymbol{\mu}, \boldsymbol{\Sigma}) = (\mathbf{x} - \boldsymbol{\mu})^\top \boldsymbol{\Sigma}^{-1} (\mathbf{x} - \boldsymbol{\mu}). \quad (3)$$

A 3D Gaussian mixture distribution is defined as

$$f_{\text{GM}}(\mathbf{x}) = \sum_{i=1}^K \pi_i \phi(\mathbf{x}|\boldsymbol{\mu}_i, \boldsymbol{\Sigma}_i), \quad (4)$$

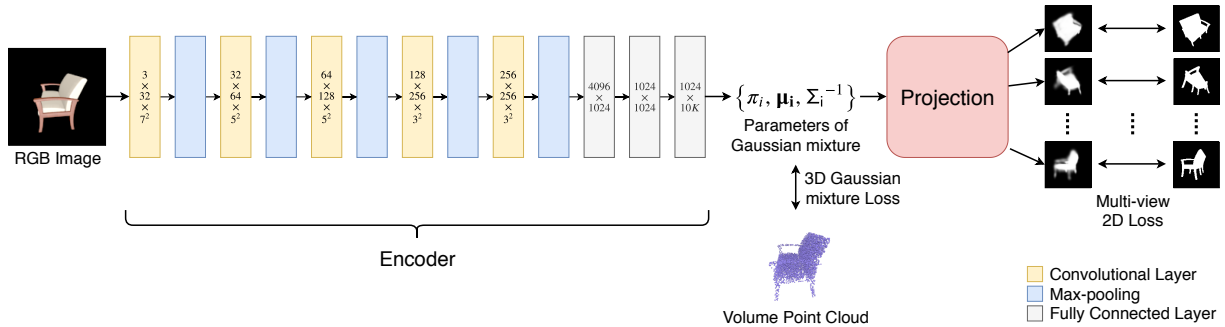


Figure 2: Overview of the proposed method. 3D-GMNet is trained by finding a Gaussian mixture that best represents the volume point cloud associated with the input image while also minimizing discrepancy in their multi-view projections. At inference time, the network outputs parameters of the Gaussian mixture shape model, which can be sampled and also converted into a surface.

where K is the number of mixture components and $\{\pi_i\}$ are the mixing coefficients that satisfy

$$\sum_{i=1}^K \pi_i = 1. \quad (5)$$

Gaussian mixtures can approximate various kinds of distributions with an appropriate K .

Surface Generation from 3D Gaussian Mixture distribution Once the density function $f_{GM}(\mathbf{x})$ is obtained, we can generate the 3D surface as follows.

Assume that we knew the volume of the object V , though it is not available in reality. The object surface is given as the isosurface of the density at

$$\tau = c \frac{1}{V}, \quad (6)$$

where the parameter c decides the level of thresholding. We approximate the unknown $\frac{1}{V}$ by the expectation of the density

$$E[f_{GM}(\mathbf{x})] = \int \{f_{GM}(\mathbf{x})\}^2 d\mathbf{x}, \quad (7)$$

since $E[f_{GM}(\mathbf{x})] = \frac{1}{V}$ holds if $f_{GM}(\mathbf{x})$ is identical to the true distribution $f(\mathbf{x})$. The parameter c is determined experimentally in the evaluations in Section 4.

By substituting Eqs. (2), (3), and (4) for Eq. (7), we obtain the following closed-form solution of the expectation

$$E[f_{GM}(\mathbf{x})] = \sum_{i=1}^K \sum_{j=1}^K \pi_i \pi_j \phi(\mathbf{x} = \boldsymbol{\mu}_i | \boldsymbol{\mu}_j, \Sigma_i + \Sigma_j). \quad (8)$$

By thresholding the target space with this value, we obtain the volumetric representation of the 3D shape, which can then be converted to a surface model using the marching cubes algorithm [15].

3.2 Network Architecture

Our 3D-GMNet outputs a set of the parameters of Gaussian mixture model, $\{\pi_i, \boldsymbol{\mu}_i, \Sigma_i^{-1}\}$. As Figure 2 depicts, it has an encoder module to predict these parameters and a projection module to render multi-view 2D silhouettes.

The numbers in the colored blocks in Figure 2 show the detail of the encoder. The encoder is composed of 5 convolutional layers, 5 max pooling layers of kernel size 2, and 3 fully-connected layers. Each of the convolution layers is followed by a batch normalization layer and a leaky ReLU activation layer. Each fully-connected layers except the last one is followed also by a leaky ReLU layer.

After these layers, 3D-GMNet introduces an output layer tailored for Gaussian mixture parameters to enforce constraints such as Eq. (5) [4, 30].

The mean $\{\boldsymbol{\mu}_i\}$ should be a 3D position in Euclidean space $\boldsymbol{\mu}_i \in \mathbb{R}^3$, and we use an identity mapping for $\boldsymbol{\mu}_i$ as

$$\boldsymbol{\mu}_i = \mathbf{a}_{\boldsymbol{\mu}_i}, \quad (9)$$

where $\mathbf{a}_{\boldsymbol{\mu}_i}$ is the corresponding output of the last layer.

In order to ensure that the coefficient $\{\pi_i\}$ satisfies Eq. (5), the output layer applies the softmax activation as

$$\pi_i = \frac{\exp(a_{\pi_i})}{\sum_j \exp(a_{\pi_j})}. \quad (10)$$

The precision matrix Σ_i^{-1} of a Gaussian component should be a symmetric positive definite matrix, and can be decomposed as $\Sigma_i^{-1} = LL^\top$ using Cholesky decomposition where L is a lower triangular matrix. Thus our network predicts $L = \{l_{ij}\}$ instead of Σ_i^{-1} where

$$l_{ij} = \begin{cases} a_{l_{ij}} & i > j, \\ \exp(a_{l_{ij}}) & i = j, \\ 0 & \text{otherwise,} \end{cases} \quad (11)$$

where $a_{l_{ij}}$ is the corresponding output of the last layer. Notice that this enforces l_{jj} to be positive so that the mapping from L to Σ_i^{-1} is bijective.

3.3 3D Gaussian Mixture Loss

As introduced in the last section, we assume that the target 3D shape is given as voxels. To quantitatively evaluate the fit of the estimated Gaussian mixture to these voxels, we use the Kullback-Leibler (KL) divergence.

In general, KL divergence between the target density $p(x)$ and the predicted density $q(x)$ is defined as

$$\text{KL}(p||q) = \int \{p(x) \log p(x) - p(x) \log q(x)\} dx. \quad (12)$$

Since $p(x) \log p(x)$ is constant, minimization of $\text{KL}(p||q)$ is equivalent to minimization of

$$- \int p(x) \log q(x) dx. \quad (13)$$

By considering the target voxels as observations from the true distribution, we can compute this efficiently with Monte Carlo sampling

$$L_{3D} = -\frac{1}{|P|} \sum_{\mathbf{x} \in P} \log f_{\text{GM}}(\mathbf{x}), \quad (14)$$

where $f_{\text{GM}}(\mathbf{x})$ is the output of our network, $\mathbf{x} \in P$ is a sample from the target density $f(\mathbf{x})$ and $|P|$ is the number of sampled points. In our training, we randomly sampled a fixed number of 3D voxels from the original target voxels for each mini batch.

We also use

$$L_{\text{dist}} = \frac{1}{K} \sum_{i=1}^K \{\text{ReLU}(|\boldsymbol{\mu}_i| - T)\}^2, \quad (15)$$

so that Gaussian components are distributed within a distance T from the object center. In this paper we use $T = 0.85$ to cover the entire object space.

3.4 Multi-view 2D Loss

We also introduce a novel multi-view 2D loss for a 3D Gaussian mixture that evaluates the consistency of its 2D projection with a given silhouette.

3.4.1 Para-perspective Projection of a Gaussian Mixture

To generate a silhouette of a 3D Gaussian mixture of Eq. (4), we use para-perspective projection [11] for each mixture component since it projects a 3D Gaussian as a 2D Gaussian. As a result, we obtain a 2D Gaussian mixture as a projection of our 3D Gaussian mixture shape representation. Note that perspective projection does not result in a Gaussian due to its nonlinearity.

Since we are only interested in object shape recovery, we can safely assume that the camera pose with respect to the object is defined by rotation about its center. Suppose we project a 3D Gaussian mixture defined in the world coordinate system to a camera of pose R . A 3D Gaussian rotated by R is given by

$$\begin{aligned} f_{\text{GM}}(\mathbf{x}; R) &= \sum_{i=1}^K \pi_i \phi(\mathbf{x} | R\boldsymbol{\mu}_i, R\Sigma_i R^\top), \\ &= \sum_{i=1}^K \pi_i \phi(\mathbf{x} | \boldsymbol{\mu}'_i, \Sigma'_i), \end{aligned} \quad (16)$$

where R is the rotation matrix transforming from the world coordinate system to the camera local coordinate system.

Para-perspective projection first defines a 3D plane Π_i located at the centroid of the object and parallel to the image plane. Since we project each of Gaussian component independently, the centroid is identical to the mean of each Gaussian $\boldsymbol{\mu}'_i = R\boldsymbol{\mu}_i$.

Suppose an oblique coordinate system centered at $\boldsymbol{\mu}'_i = R\boldsymbol{\mu}_i$ and whose x and y axes are identical to the original Euclidean system but its third w axis is the direction from the camera center (*i.e.*, the origin of the camera coordinate system) to the centroid. Transforming a 3D point \mathbf{x} in the

camera coordinate system to a 3D point $\mathbf{y} = (u, v, w)^\top$ in this oblique system can then be described by

$$\mathbf{x} = (\mathbf{e}_x^\top, \mathbf{e}_y^\top, \boldsymbol{\mu}'^\top) \mathbf{y} = M_i \mathbf{y} \quad (17)$$

$$\mathbf{y} = M_i^{-1} \mathbf{x}, \quad (18)$$

where $\mathbf{e}_x = (1, 0, 0)^\top$ and $\mathbf{e}_y = (0, 1, 0)^\top$. Therefore, the Gaussian of Eq. (16) is transformed to a Gaussian of parameters

$$\boldsymbol{\mu}'' = \boldsymbol{\mu}', \quad \Sigma''^{-1} = M_i^\top \Sigma_i^{-1} M_i, \quad (19)$$

and the parallel projection to the plane Π_i is given by marginalizing this Gaussian $\phi(\mathbf{x} | \boldsymbol{\mu}'', \Sigma'')$ in the w direction

$$\boldsymbol{\mu}''' = (\mathbf{e}_x^\top, \mathbf{e}_y^\top) \boldsymbol{\mu}'', \quad \Sigma'''^{-1} = \begin{pmatrix} s_{00} - \frac{s_{02}^2}{s_{22}} & s_{01} - \frac{s_{12}s_{02}}{s_{22}} \\ s_{10} - \frac{s_{12}s_{02}}{s_{22}} & s_{11} - \frac{s_{12}^2}{s_{22}} \end{pmatrix} \quad (20)$$

where s_{ij} denotes the (i, j) element of Σ''^{-1} . By applying a 2D affine transform from the plane Π_i to the image plane, we obtain the 2D Gaussian on the image plane as

$$\boldsymbol{\mu}'''' = \frac{\boldsymbol{\mu}'''}{z_i}, \quad \Sigma''''^{-1} = \frac{1}{z_i^2} \Sigma'''^{-1}, \quad (21)$$

where z_i is the depth of the centroid, *i.e.*, the z element of $\boldsymbol{\mu}'_i$.

As a result, the para-perspective projection of a 3D Gaussian of Eq. (16) is given by

$$d(\mathbf{x}) = \sum_{i=1}^K \pi_i \phi_{2D}(\mathbf{x} | \boldsymbol{\mu}''''_i, \Sigma''''_i), \quad (22)$$

where $\phi_{2D}(\cdot)$ denotes a 2D Gaussian of the form

$$\phi_{2D}(\mathbf{x} | \boldsymbol{\mu}''''_i, \Sigma''''_i) = \frac{1}{2\pi |\Sigma''''_i|^{\frac{1}{2}}} \exp\left(-\frac{1}{2} g(\mathbf{x} | \boldsymbol{\mu}''''_i, \Sigma''''_i)\right) \quad (23)$$

This para-perspective projection is differentiable and denoted as the projection module in Figure 2.

3.4.2 Silhouette Loss

In order to evaluate the consistency between the projected 2D Gaussian mixture of Eq. (22) and the ground truth silhouette $s(\mathbf{x}) \in [0, 1]$, we generate a pseudo soft silhouette $\hat{s}(\mathbf{x})$ from Eq. (22).

Given a random sampling of Q points from the 2D probability density function $d(\mathbf{x})$ of Eq. (22), the probability of observing at least a point out of the Q points at a pixel position \mathbf{x} is given by

$$\hat{s}(\mathbf{x}) = 1 - \{1 - d(\mathbf{x})\}^Q. \quad (24)$$

By approximating the silhouette generated from the probability density function by this $\hat{s}(\mathbf{x})$, we define an L2 loss

$$L_{\text{sil}}(\hat{s}(\mathbf{x}), s(\mathbf{x})) = \sum_{\mathbf{x}} \{\hat{s}(\mathbf{x}) - s(\mathbf{x})\}^2, \quad (25)$$

as our silhouette loss. In the experiments, we determined Q using validation data ($Q = 65536$).

3.5 Training

As Figure 2 illustrates, given a 2D image of a 3D object as the input, the 3D-GMNet estimates the parameters of a 3D Gaussian mixture that represents the 3D shape of the target in the camera coordinate system. For this, the target voxels used in the 3D Gaussian mixture loss (Section 3.3) is transformed according to the ground truth camera pose of the input image beforehand. Once the GMM parameters are estimated, the network renders 2D silhouettes from N random viewpoints and evaluates the multi-view 2D loss (Section 3.4). This process also requires N ground truth camera poses in addition to their ground truth silhouettes. In the experiments, we use $N = 4$.

4 Experimental Results

We evaluate our method for the task of class-specific single-image 3D reconstruction. We first describe data and metrics used for our experiments and then detail quantitative evaluation on synthetic and real images. In addition, we show two applications of our method, a 3D pose alignment of reconstructed 3D shapes and an automatic level-of-computation, both of which demonstrate advantages of a 3D Gaussian mixture shape representation that conventional methods do not have.

Data To conduct thorough quantitative evaluation, we synthesized multi-view images and 3D point clouds of 3D models in ShapeNet [5]. Each 3D model in ShapeNet has

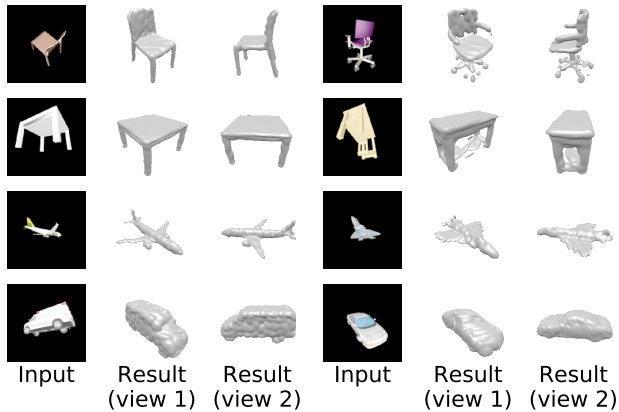


Figure 3: Results of class-specific single image 3D reconstruction for 4 object categories where the number of mixture components K is 256. The marching cubes algorithm [15] is used to extract the surface. Since our network estimates the 3D Gaussian mixture shape in the camera coordinate system, the results are transformed first to the world coordinate system using the ground truth pose parameter of the camera and then projected to the novel views view 1 and view 2 for evaluation.

a polygon CAD model and its volume data. For each polygon model, multi-view RGB images are rendered from random 100 viewpoints at a unit distance from the model using a tessellated icosahedron. To normalize the apparent size of the model in the rendered images, the distance is adjusted on a per-model basis as the diagonal size of the object bounding box. The virtual camera is configured as 128×128 resolution and 68° field-of-view. We train and evaluate our network for 4 object categories, namely *Chair*, *Car*, *Airplane* and *Table*.

For real images, we evaluate our method using real chair images in Pix3D Dataset [25]. We remove images in which the object is partly in the image or occluded by other objects for simplicity. Occlusion handling will be addressed in future work. We resize and crop images using manually annotated 2D masks.

Evaluation Metrics Following [25], we use three metrics for evaluation: intersection of union (IoU), earth mover’s distance (EMD), and chamfer distance (CD). IoU evaluates the coverage of the estimated volume w.r.t. the ground truth volume, using the Gaussian mixture vox-

Table 1: Quantitative evaluation of multi-view silhouette loss.

	CD	EMD	IoU
3D	0.0866	0.0923	0.466
3D + MV	0.0842	0.0889	0.482

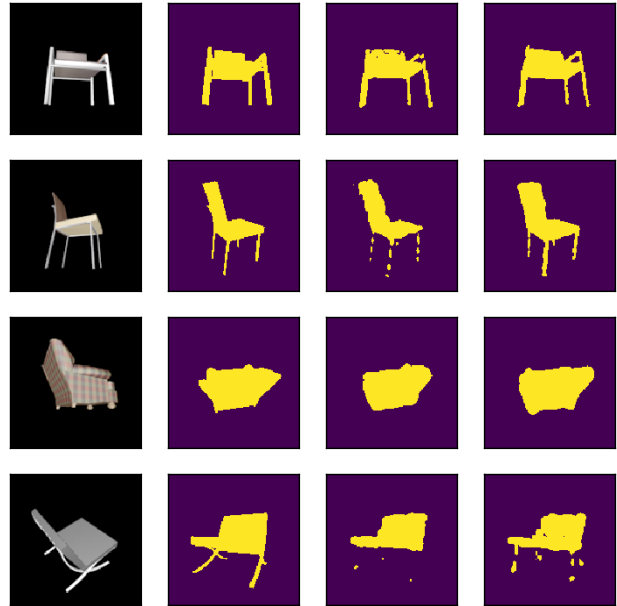


Figure 4: Input image, ground truth silhouette, results without and with silhouette loss. Silhouette loss improves completeness.

elization in Section 3.1. Higher IoU means better reconstruction results. EMD and CD evaluate geodesic and shortest distances between two surfaces via point clouds sampled on them. As described in [25], we uniformly sampled points on the estimated and the ground truth surface to generate a dense point cloud, and then randomly sampled 1024 points from the point cloud. They are scaled to fit a unit cube for normalization for EMD and

Table 2: Quantitative evaluation of generated silhouette with and without silhouette loss.

	MSE	CD_{acc}	CD_{comp}
3D	0.0487	0.574	0.419
3D + MV	0.0468	0.558	0.317

CD calculation. We used the implementation by Sun *et al.* [25].

To further analyze the effect of silhouette loss, we generate 128×128 silhouette images of the reconstructed 3D shape. For quantitative evaluation, we use MSE, CD_{acc} , and CD_{comp} . MSE is the pixel-wise squared error of the silhouette images. CD_{acc} is the average distance to the ground truth silhouette for each pixel in the generated silhouette. CD_{comp} is the one from the ground truth to the generated silhouette.

Training Parameters We use the Adam optimizer with learning rate of 10^{-4} . The mini batch size is set to 64. Training loss is averaged in each mini batch. We use 80% of the 3D models in ShapeNet for training and 10% for validation. The rest of 10% is kept for evaluation.

4.1 Single Image 3D Reconstruction

Figure 3 shows predicted 3D models. Given an input image shown in the first and fourth columns from left, our 3D-GMNet estimates its 3D shape as a 3D Gaussian mixture. The rest of the columns show renderings of the estimated 3D Gaussian mixture shape as a surface model (Section 3.1) from different viewpoints. The renderings from the novel views demonstrate qualitatively that the proposed 3D-GMNet can estimate the full 3D shape from a single image successfully.

Contribution of Silhouette Loss Table 1 shows quantitative evaluation of multi-view silhouette loss. The results show that the silhouette loss reduces 3D shape reconstruction errors.

Figure 4 shows silhouettes of reconstructed 3D shapes with/without the silhouette loss. Table 2 shows quantitative evaluation of the silhouette. Though the silhouette loss is computed by using pseudo silhouettes, the quality of the actual silhouette is improved. Especially, the completeness (CD_{comp}) improves drastically.

Number of Gaussian Components Figure 5 shows reconstruction results with different numbers of mixture components K . Figure 7 reports the reconstruction errors. We can observe that though reconstructions with higher

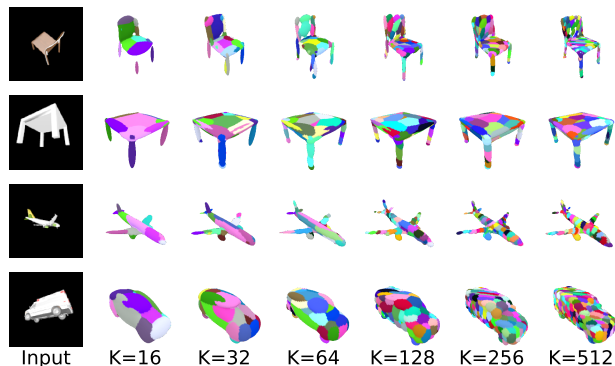


Figure 5: 3D shapes estimated with different numbers of Gaussian components. The color indicates the distinct Gaussian component the point belongs to.

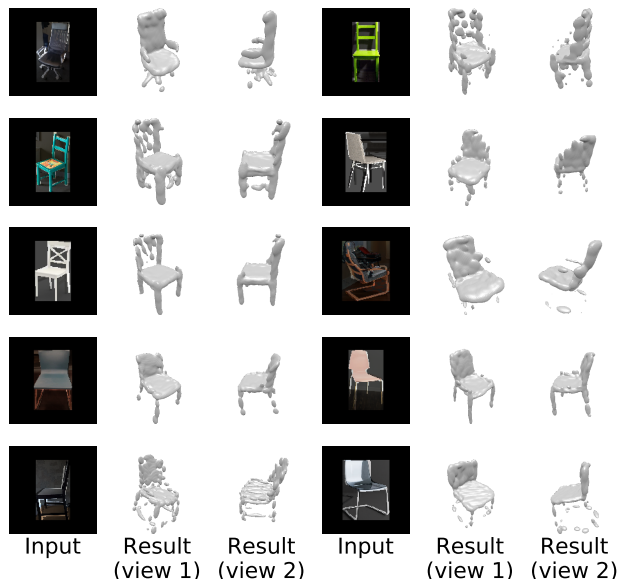


Figure 6: Reconstruction from real images in Pix3D dataset [25].

K results in a detailed reconstruction, those with lower K also approximates the 3D shape accurately.

3D Reconstruction from Real Images Figure 6 and Table 3 show single-image 3D reconstruction results with real images in Pix3D dataset [25]. From these results We can conclude that the reconstruction accuracy of our 3D-

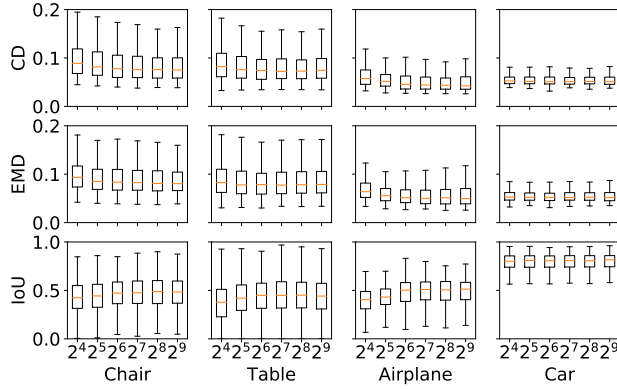


Figure 7: Quantitative results at different number of the components K .

GMNet is comparable to the state-of-the-art methods.

4.2 3D Pose Alignment

As described in Section 3.5, our 3D-GMNet generates the shape from the input camera local coordinate system. This suggests that given two images of a single object from different viewpoints, our 3D-GMNet generates a 3D shape described in different coordinate systems, and hence we can estimate the relative pose of the cameras via aligning the estimated 3D shapes.

A challenge here is the view-dependent assignment of Gaussian components on representing a same 3D object shape from different views, and we cannot directly consider component-wise correspondences. This is because our loss functions only require the Gaussian mixture represent the object shape as a whole and the network can change the assignment of each Gaussian component freely for each image.

We solve this by aligning the covariance matrices of Gaussian mixtures from different viewpoints. The covariance matrix of a Gaussian mixture (Eq. (4)) is given by

$$\Sigma_{\text{GM}} = \sum_{i=1}^K \pi_i \left(\Sigma_i + (\boldsymbol{\mu}_i - \boldsymbol{\mu}_{\text{GM}})(\boldsymbol{\mu}_i - \boldsymbol{\mu}_{\text{GM}})^\top \right),$$

where $\boldsymbol{\mu}_{\text{GM}} = \sum_{i=1}^K \pi_i \boldsymbol{\mu}_i$. We then estimate the rotation via diagonalization with its eigenvectors sorted in descending order according to the magnitude of the corresponding eigenvalues. The correspondence based on the

Table 3: Quantitative evaluation of single image 3D reconstructions using real images in Pix3D dataset [25]. Top 7 rows are the results reported by Sun *et al.* [25]. The last line is the result with a data augmentation in the training ShapeNet data so that the object appears in different scales in the image as Pix3D images do.

	IoU	EMD	CD
3D-R2N2 [6]	0.136	0.211	0.239
PSGN [7]	N/A	0.216	0.200
3D-VAE-GAN [32]	0.171	0.176	0.182
DRC [28]	0.265	0.144	0.160
MarrNet [31]	0.231	0.136	0.144
AtlasNet [9]	N/A	0.128	0.125
Pix3D [25]	0.287	0.120	0.119
Ours	0.250	0.131	0.134
Ours*	0.259	0.129	0.130

order of eigenvalues has a sign ambiguity on each of the eigenvectors. To find the correct signs, we evaluate the rotation that minimizes the L_2 distance between two Gaussian mixtures:

$$\int \left(f_{\text{GM}}^{(1)}(\mathbf{x}) - f_{\text{GM}}^{(2)}(\mathbf{x}) \right)^2 d\mathbf{x} = \sum_{i,j} \Phi^{(1,1)}(i,j) + \sum_{i,j} \Phi^{(2,2)}(i,j) - 2 \sum_{i,j} \Phi^{(1,2)}(i,j), \quad (26)$$

where

$$\begin{aligned} \Phi^{(a,b)}(i,j) &= \pi_i^{(a)} \pi_j^{(b)} \int \phi_i^{(a)}(\mathbf{x}) \phi_j^{(b)}(\mathbf{x}) d\mathbf{x} \\ &= \pi_i^{(a)} \pi_j^{(b)} \phi \left(\mathbf{x} = \boldsymbol{\mu}^{(a)} | \boldsymbol{\mu}^{(b)}, \boldsymbol{\Sigma}^{(a)} + \boldsymbol{\Sigma}^{(b)} \right). \end{aligned} \quad (27)$$

Figure 8 shows the alignment results. The results show that our method can provide reasonable pose alignments without explicit point cloud generation.

4.3 Level-of-Detail Computation

Figure 9 demonstrates a level-of-detail visualization of Gaussian mixture representation. Given an input image (the leftmost column), our network with $K = 512$ infers a Gaussian mixture representation of its 3D shape

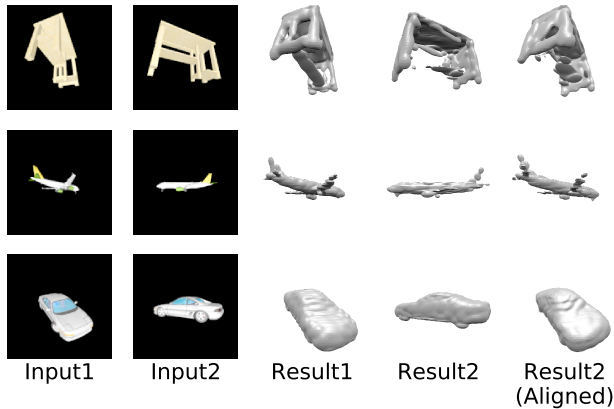


Figure 8: The result of 3D pose alignment. The first 2 columns are input images and the next 2 columns are the corresponding 3D reconstruction results, which are viewer-centered. The last column is the alignment result. The poses of the reconstruction results in the 4th column are aligned to the poses of the 3rd column’s.

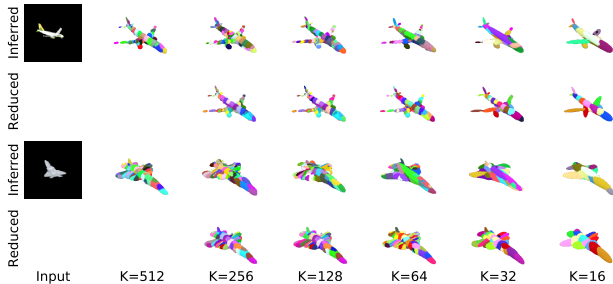


Figure 9: Level-of-detail computation. The first and the third rows show the estimated 3D shape originally trained for $K = 16, 32, \dots, 512$ (c.f. Figure 5). The second and the fourth rows show results of Gaussian mixture reduction from $K = 512$ to $K = 16, 32, \dots, 256$.

(the second column). By applying Gaussian mixture reduction [22], we obtain level-of-detail visualizations as shown in the second and the fourth rows. Compared with the 3D shapes estimated by 3D-GMNet originally trained with the corresponding number of components (the first and the third rows), this automatic computation yields reasonable approximations.

5 Conclusion

We proposed 3D-GMNet for single image 3D object shape reconstruction with a Gaussian mixture representation. The proposed network utilizes the 3D loss and the multi-view 2D loss to evaluate the fitting of the estimated Gaussian mixture to the 3D ground truth shape and its 2D silhouettes. Experimental results show that our 3D-GMNet successfully estimates the object 3D shape as a compact Gaussian mixture representation, even with a lower number of components, while maintaining reconstruction accuracy comparable to state-of-the-art results.

Acknowledgement

This work was in part supported by JSPS KAKENHI 17K20143 and JST PREST JPMJPR1858.

References

- [1] S. Agarwal, Y. Furukawa, N. Snavely, I. Simon, B. Curless, S. M. Seitz, and R. Szeliski. Building rome in a day. *Communications of the ACM*, 54(10):105–112, 2011. 1
- [2] A. Agrawal, R. Raskar, and R. Chellappa. What is the range of surface reconstructions from a gradient field? In *Proc. ECCV*, pages 578–591. Springer, 2006. 1
- [3] N. Alldrin, T. Zickler, and D. Kriegman. Photometric stereo with non-parametric and spatially-varying reflectance. In *Proc. CVPR*, pages 1–8. IEEE, 2008. 1
- [4] C. M. Bishop. Mixture density networks. Technical report, Aston University, 1994. 3, 4
- [5] A. X. Chang, T. Funkhouser, L. Guibas, P. Hanrahan, Q. Huang, Z. Li, S. Savarese, M. Savva, S. Song, H. Su, et al. Shapenet: An information-rich 3d model repository. *arXiv:1512.03012*, 2015. 1, 6
- [6] C. B. Choy, D. Xu, J. Gwak, K. Chen, and S. Savarese. 3d-r2n2: A unified approach for single and multi-view 3d object reconstruction. In *Proc. ECCV*, 2016. 1, 2, 3, 9
- [7] H. Fan, H. Su, and L. J. Guibas. A point set generation network for 3d object reconstruction from a single image. In *Proc. CVPR*, July 2017. 1, 2, 3, 9
- [8] P. Favaro, S. Soatto, M. Burger, and S. J. Osher. Shape from defocus via diffusion. *TPAMI*, 30(3):518–531, 2008. 1
- [9] T. Groueix, M. Fisher, V. G. Kim, B. Russell, and M. Aubry. AtlasNet: A Papier-Mâché Approach to Learning 3D Surface Generation. In *Proc. CVPR*, 2018. 2, 9

- [10] K. Häming and G. Peters. The structure-from-motion reconstruction pipeline - a survey with focus on short image sequences. *Kybernetika*, 46(5):926–937, 2010. 1
- [11] R. Hartley and A. Zisserman. *Multiple View Geometry in Computer Vision*. Cambridge University Press, New York, NY, USA, 2 edition, 2003. 5
- [12] C. Hernández, G. Vogiatzis, G. J. Brostow, B. Stenger, and R. Cipolla. Non-rigid photometric stereo with colored lights. In *Proc. ICCV*, pages 1–8. IEEE, 2007. 1
- [13] L. Jiang, S. Shi, X. Qi, and J. Jia. Gal: Geometric adversarial loss for single-view 3d-object reconstruction. In *Proc. ECCV*, 2018. 1, 2, 3
- [14] H. Kato, Y. Ushiku, and T. Harada. Neural 3d mesh renderer. In *Proc. CVPR*, 2018. 2, 3
- [15] T. Lewiner, H. Lopes, A. W. Vieira, and G. Tavares. Efficient implementation of marching cubes’ cases with topological guarantees. *Journal of graphics tools*, 8(2):1–15, 2003. 4, 7
- [16] C.-H. Lin, C. Kong, and S. Lucey. Learning efficient point cloud generation for dense 3d object reconstruction. In *Proc. AAAI*, 2018. 1, 2, 3
- [17] L. Mescheder, M. Oechsle, M. Niemeyer, S. Nowozin, and A. Geiger. Occupancy networks: Learning 3d reconstruction in function space. In *Proc. CVPR*, 2019. 2
- [18] S. Nayar and Y. Nakagawa. Shape from focus. *TPAMI*, (8):824–831, 1994. 1
- [19] C. Niu, J. Li, and K. Xu. Im2struct: Recovering 3d shape structure from a single rgb image. In *Proc. CVPR*, 2018. 2
- [20] J. J. Park, P. Florence, J. Straub, R. Newcombe, and S. Lovegrove. DeepSDF: Learning continuous signed distance functions for shape representation. In *Proc. CVPR*, 2019. 2
- [21] D. Paschalidou, A. O. Ulusoy, and A. Geiger. Superquadrics revisited: Learning 3d shape parsing beyond cuboids. In *Proc. CVPR*, 2019. 2
- [22] A. R. Runnalls. Kullback-leibler approach to gaussian mixture reduction. *IEEE Transactions on Aerospace and Electronic Systems*, 43(3):989–999, July 2007. 10
- [23] D. Scharstein and R. Szeliski. A taxonomy and evaluation of dense two-frame stereo correspondence algorithms. *IJCV*, 47(1-3):7–42, 2002. 1
- [24] J. L. Schonberger and J.-M. Frahm. Structure-from-motion revisited. In *Proc. CVPR*, pages 4104–4113, 2016. 1
- [25] X. Sun, J. Wu, X. Zhang, Z. Zhang, C. Zhang, T. Xue, J. B. Tenenbaum, and W. T. Freeman. Pix3d: Dataset and methods for single-image 3d shape modeling. In *Proc. CVPR*, 2018. 7, 8, 9
- [26] K. Tateno, F. Tombari, I. Laina, and N. Navab. Cnn-slam: Real-time dense monocular slam with learned depth prediction. In *Proc. CVPR*, pages 6243–6252, 2017. 1
- [27] S. Tulsiani, H. Su, L. J. Guibas, A. A. Efros, and J. Malik. Learning shape abstractions by assembling volumetric primitives. In *Proc. CVPR*, 2017. 2
- [28] S. Tulsiani, T. Zhou, A. A. Efros, and J. Malik. Multi-view supervision for single-view reconstruction via differentiable ray consistency. In *Proc. CVPR*, July 2017. 9
- [29] N. Wang, Y. Zhang, Z. Li, Y. Fu, W. Liu, and Y.-G. Jiang. Pixel2mesh: Generating 3d mesh models from single rgb images. In *Proc. ECCV*, 2018. 1, 2, 3
- [30] P. Williams. Using neural networks to model conditional multivariate densities. *Neural computation*, 8:843–854, 06 1996. 3, 4
- [31] J. Wu, Y. Wang, T. Xue, X. Sun, W. T. Freeman, and J. B. Tenenbaum. MarrNet: 3D Shape Reconstruction via 2.5D Sketches. In *Proc. NIPS*, 2017. 1, 2, 9
- [32] J. Wu, C. Zhang, T. Xue, B. Freeman, and J. Tenenbaum. Learning a probabilistic latent space of object shapes via 3d generative-adversarial modeling. In *Proc. NIPS*, pages 82–90. Curran Associates, Inc., 2016. 9
- [33] X. Yan, J. Yang, E. Yumer, Y. Guo, and H. Lee. Perspective transformer nets: Learning single-view 3d object reconstruction without 3d supervision. In *Proc. NIPS*, pages 1696–1704. Curran Associates, Inc., 2016. 3